

Isotropic negative thermal expansion and its mechanism in tetracyanidoborate salt $CuB(CN)_4$

Chunyan Wang(王春艳), Qilong Gao(高其龙), Andrea Sanson, and Yu Jia(贾瑜)
Citation: Chin. Phys. B, 2022, 31 (**6**): 066501. DOI: 10.1088/1674-1056/ac6019
Journal homepage: http://cpb.iphy.ac.cn; http://iopscience.iop.org/cpb

What follows is a list of articles you may be interested in

Near-zero thermal expansion in β-$CuZnV_2O_7$ in a large temperature range

Yaguang Hao(郝亚光), Hengli Xie(谢恒立), Gaojie Zeng(曾高杰), Huanli Yuan(袁焕丽), Yangming Hu(胡杨明), Juan Guo(郭娟), Qilong Gao(高其龙), Mingju Chao(晁明举), Xiao Ren(任霄), and Er-Jun Liang(梁二军)
Chin. Phys. B, 2022, 31 (**4**): 046502. DOI: 10.1088/1674-1056/ac3393

Zero thermal expansion in metal-organic framework with imidazole dicarboxylate ligands

Qilong Gao(高其龙), Yixin Jiao(焦怡馨), and Gang Li(李纲)
Chin. Phys. B, 2022, 31 (**4**): 046501. DOI: 10.1088/1674-1056/ac3ecf

Effects of W^{6+} occupying Sc^{3+} on the structure, vibration, and thermal expansion properties of scandium tungstate

Dongxia Chen(陈冬霞), Qiang Sun(孙强), Zhanjun Yu(于占军), Mingyu Li(李明玉), Juan Guo(郭娟), Mingju Chao(晁明举), and Erjun Liang(梁二军)
Chin. Phys. B, 2021, 30 (**6**): 066501. DOI: 10.1088/1674-1056/abd7d4

Negative thermal expansion in NbF_3 and $NbOF_2$: A comparative theoretical study

Mingyue Zhang(张明月), Chunyan Wang(王春艳), Yinuo Zhang(张一诺), Qilong Gao(高其龙), and Yu Jia(贾瑜)
Chin. Phys. B, 2021, 30 (**5**): 056501. DOI: 10.1088/1674-1056/abe376

Negative thermal expansion of Ca_2RuO_4 with oxygen vacancies

Sen Xu(徐森), Yangming Hu(胡杨明), Yuan Liang(梁源), Chenfei Shi(史晨飞), Yuling Su(苏玉玲), Juan Guo(郭娟), Qilong Gao(高其龙), Mingju Chao(晁明举), Erjun Liang(梁二军)
Chin. Phys. B, 2020, 29 (**8**): 086501. DOI: 10.1088/1674-1056/ab8a36

RAPID COMMUNICATION

Isotropic negative thermal expansion and its mechanism in tetracyanidoborate salt $CuB(CN)_4$

Chunyan Wang(王春艳)[1,2,3], Qilong Gao(高其龙)[1,†], Andrea Sanson[4], and Yu Jia(贾瑜)[2,3]

[1] *Key Laboratory of Materials Physics of Ministry of Education, International Laboratory for Quantum Functional Materials of Henan, and School of Physics and Microelectronics, Zhengzhou University, Zhengzhou* 450052, *China*

[2] *Key Laboratory of Special Functional Materials of Ministry of Education, and School of Materials Science and Engineering, Henan University, Kaifeng* 475004, *China*

[3] *Key Laboratory for Quantum Materials and Center for Topological Functional Materials, Henan University, Kaifeng* 475004, *China*

[4] *Department of Physics and Astronomy, University of Padova, Padova I*-35131, *Italy*

(Received 29 January 2022; revised manuscript received 26 February 2022; accepted manuscript online 23 March 2022)

The control of thermal expansion is essential in applications where thermal stability is required from fiber optics coatings, high performance fuel cell cathodes to tooth fillings. Negative thermal expansion (NTE) materials, although rare, are fundamental for this purpose. This work focuses on studying tetracyanidoborate salt $CuB(CN)_4$, an interesting cubic-structure material that displays large isotropic NTE. A joint study of synchrotron x-ray diffraction, temperature-dependent Raman spectroscopy, and lattice dynamics calculations was conducted, showing that not only low-frequency optical modes (transverse thermal vibrations of N and C atoms) but also the acoustic modes (the vibrations of Cu atoms as a collective torsion of the neighboring atoms), contribute to NTE. As a result, new insights were gained into the NTE mechanism of $CuB(CN)_4$ and related framework materials.

Keywords: negative thermal expansion, Prussian blue analogues, crystal structure, phonons

PACS: 65.40.De, 61.66.Fn, 63.20.D−, 78.30.−j **DOI:** 10.1088/1674-1056/ac6019

After the discovery that ZrW_2O_8 displays strong negative thermal expansion (NTE) over a wide temperature range,[1,2] the interest in NTE has increased considerably due to its promising applications in different engineering fields from fiber optics coatings, high performance fuel cell cathodes to tooth fillings.[3,4] Since then different NTE materials were found out[5–8] and classified into two classes according to the NTE mechanism:[9–13] phonons driven open-framework materials, such as oxides,[1,3,14,15] fluorides,[16,17] cyanides/Prussian blue analogues (PBAs)[18–21] and MOFs;[22,23] electronic-related driven materials, such as magnetovolume effect in manganese nitrides[24,25] and Invar alloys,[26,27] ferroelectrovolume effect in $PbTiO_3$,[28] charge transfer in $BiNiO_3$,[29] metal–insulating transition in Ca_2RuO_4.[30] Other examples can be found in the review papers.[5,7,31,32]

The isotropic NTE materials are very interesting since they can reduce the thermal stress in composites, but, unfortunately, their number is very limited. ZrW_2O_8 and ScF_3 are the most popular isotropic NTE materials. Their structural flexibility, directly connected to the transverse thermal vibrations of bridging atoms, plays a key role in NTE behavior.[33,34] Interestingly, Sanson[6] related the behavior of the transverse thermal vibrations and therefore of thermal expansion to the length of the crystallographic lattice parameter. Recently, Gao *et al.*[35] adopted the concept of "average atomic volume (AAV)" to evaluate the structural flexibility and to qualitatively predict the thermal expansion behavior. Based on these ideas, some new negative and zero thermal expansion materials[36,37] were found out, including the $CuB(CN)_4$ NTE material presented in this work.

NTE in open-framework materials is typically related to the presence of low-frequency phonons with negative Grüneisen parameters, but intriguing differences, based on their structural features, characterize each material and some aspects remain controversial. This is the case, for example, of zirconium tungstate ZrW_2O_8, where the origin of NTE has been widely debated in the years,[28,38] or the case of $M^{II}(CN)_2$ (M = Zn, Cd) cyanides, where two dominant optical modes seem to contribute mainly to NTE,[39] in contrast to other studies where NTE is attributed to transverse acoustic modes.[40] The isotropic NTE behavior of cubic $CuB(CN)_4$ was recently reported in Ref. [30], but no information is known about the origin of NTE. From the structure analysis reported in 2005 by Togo *et al.*,[41] the AAV of $CuB(CN)_4$ is close to the value 16 Å^3, which is the critical point from positive to negative thermal expansion reported in Ref. [30]. $CuB(CN)_4$ is isostructural with $AgB(CN)_4$ and belongs to the $Zn(CN)_2$-type structure. The C and N atoms in $CuB(CN)_4$ form linear B–C ≡ N–Cu linkages, a suitable

†Corresponding author. E-mail: qilonggao@zzu.edu.cn

© 2022 Chinese Physical Society and IOP Publishing Ltd

condition that favors the NTE mechanism. In this work, we aim to shed light on the isotropic NTE mechanism observed in $CuB(CN)_4$ through a joint study of high-resolution synchrotron x-ray diffraction (SXRD), temperature-dependent Raman spectroscopy and first principles calculations based on density functional theory.

The crystal structure of $CuB(CN)_4$ was investigated by high-resolution SXRD (the detailed sample characterizations in supporting information) and the refined structure indicates that $CuB(CN)_4$ has a cubic structure with space group *P*-43*m* (215) and lattice parameter $a = 5.40555(8)$ Å at 300 K, in agreement with a previous study.[36] Similar to $AgB(CN)_4$, the $CuB(CN)_4$ structure is formed by CuN_4 and BC_4 tetrahedra, bridged through CN units (Fig. 1). The value of the AAV for $CuB(CN)_4$, calculated by equation $AAV = V/(Z \times N)$ where V is the unit cell volume ($V = 157.95$ Å^3), Z is the cell formula units ($Z = 1$) and N is the number of atoms in the chemical formula ($N = 10$), is estimated to be about 15.8 Å^3, hence close to the critical point for the switch from negative to positive thermal expansion.[30]

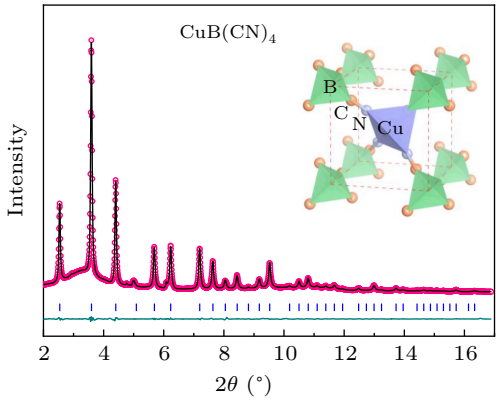


Fig. 1. SXRD structure refinement of $CuB(CN)_4$ at 300 K. The inset shows a sketch of the cubic structure, space group *P*-43*m*.

The thermal expansion of $CuB(CN)_4$ was determined by temperature-dependent SXRD. Interestingly, it displays an isotropic NTE behavior with linear thermal expansion coefficient $\alpha_l = -9.15 \times 10^{-6}$ K^{-1} in the temperature range 100–400 K. This experimental result is consistent with our DFT calculations, as shown in Fig. 2(a). It can be observed that the NTE of $CuB(CN)_4$ is much weaker than that of isostructural $AgB(CN)_4$ (-40×10^{-6} K^{-1}, 100–600 K), in agreement with the smaller value of the AAV.

It is widely accepted that the NTE in open-framework materials is driven by the transverse thermal vibrations of bridging atoms.[4] Here, the atomic mean-square displacements (MSDs) parallel (||) and perpendicular ($\perp$) to the Cu–N ≡ C–B bond direction have been determined by SXRD analysis for the C and N atoms. As shown in Fig. 2(b), the perpendicular $MSDs_\perp$ of both N and C atoms are much larger than the parallel $MSDs_\parallel$ ones, thus indicating the presence of large anisotropy. In particular, the perpendicular $MSDs_\perp$ of N atoms are larger than that of C atoms. This suggests that the NTE in $CuB(CN)_4$ mainly comes from the transverse thermal vibrations of N atoms, similarly to other NTE PBAs such as $TiCo(CN)_6$[42] and $YFe(CN)_6$.[10]

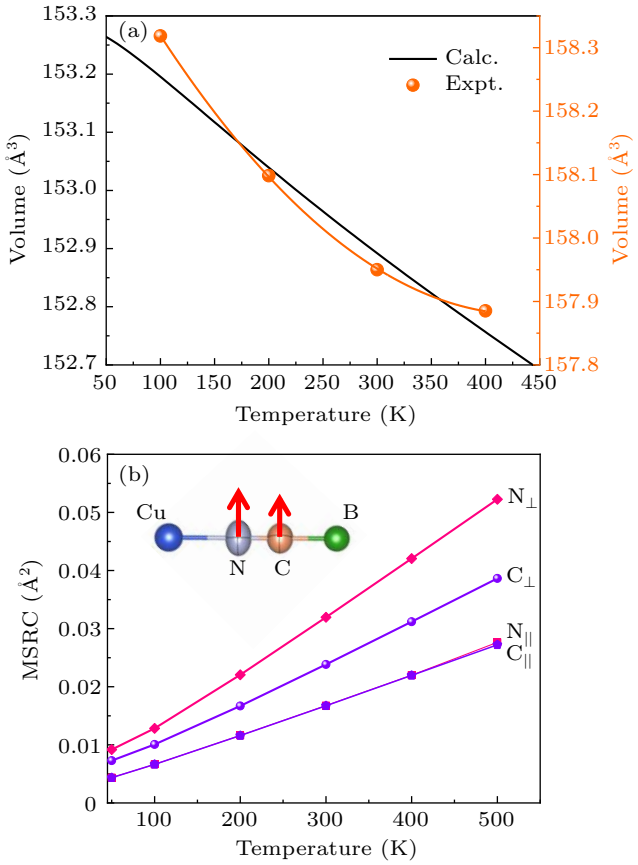


Fig. 2. (a) Temperature dependence of the lattice volume of $CuB(CN)_4$ measured by SXRD and evaluated by first-principle calculations. (b) Parallel and perpendicular MSDs of N and C atoms calculated by our first-principles calculations. The inset represents the thermal ellipsoids of N and C atoms.

Additional information on the lattice dynamics and NTE mechanism can be obtained by temperature-dependent Raman spectroscopy combined with first-principles calculations. On the basis of the factor group analysis, $2A_1 + 2E + 2F_1 + 5F_2$ vibrational modes at the Γ-point of the Brillouin zone are expected, where the F_1 and F_2 modes are triple degenerate modes and the E modes are double degenerate modes. The E and A_1 modes are Raman active, whereas the F_2 modes are both infrared and Raman active and the remaining F_1 modes are inactive (silent). Accordingly, nine Raman active modes are expected in $CuB(CN)_4$. Figure 3(a) shows the (unpolarized) Raman spectrum collected in $CuB(CN)_4$ at 300 K, Table 1 reports the calculated phonon frequencies at the Γ-point.

According to our first-principles calculations, the experimental Raman peaks at about 160 cm^{-1} and 277 cm^{-1} correspond to the symmetric and anti-symmetric rocking vibrations of N-BC_4 groups, respectively, while the Raman peaks

at about 200 cm^{-1}, 508 cm^{-1} and 520 cm^{-1} correspond to the in-plane bending of B–C ≡ N bonds. The Raman peaks at ∼ 572 cm^{-1} and ∼ 951/958/989 cm^{-1} refer to the symmetric and anti-symmetric stretching vibrations of B-C bonds, respectively, and, finally, the two Raman peaks at about 2300 cm^{-1} can be attributed to the stretching vibrations of the C ≡ N bonds. We guess here that the presence of three Raman peaks at 951/958/989 cm^{-1}, also observed in Ref. [36], is the result of the degeneracy removal of the F_2 (R, IR) mode calculated at ∼ 941 cm^{-1}. This statement is corroborated by the IR bands observed at the same frequency position.[43] Analogous conclusion can be hypothesized for the weak Raman peak detected at ∼ 2209 cm^{-1}, also visible in Ref. [36], since at the same position there is again an IR peak. A very small peak seems visible also at ∼ 2228 cm^{-1} in the lowest-temperature spectra.

Table 1. Calculated and observed vibrational modes of $CuB(CN)_4$ at the Γ-point. The quantity $\frac{1}{\omega_i}\left(\frac{\partial\omega_i}{\partial T}\right)_P$ has been estimated from the temperature dependence of Raman spectra, while the Grüneisen parameters γ_i have been determined from first-principles calculations.

Modes	Frequency Calc. (cm^{-1})	Raman intensity Calc. (arb. units)	Frequency Exp. 100 K (cm^{-1})	$\frac{1}{\omega_i}\left(\frac{\partial\omega_i}{\partial T}\right)_P$ ($\times10^{-5}$ K^{-1})	γ_i	Assignment
F_1	93.5	–			−5.6	Trans. C ≡ N
F_2(R, IR)	173.3	101.4	160	−16.1	2.45	ρ_s(N–BC_4)
E(R)	218.4	0.3	200	−2.0	0.16	δ(B–C ≡ N)
F_2(R, IR)	295.7	30.1	277	−13.9	1.14	ρ_a(N–BC_4)
F_1	327.8	–	–	–	−1.45	Libr. C ≡ N
F_2(R, IR)	494.5	58.0	508	−0.7	0.33	δ(B–C ≡ N)
E(R)	504.6	10.3	520	−0.3	−0.25	δ(B–C ≡ N)
A_1(R)	578.2	124.4	572	−3.8	1.88	ν_s(BC)
F_2(R, IR)	940.9	2.9	951	−1.5	0.89	ν_a(BC)
			958	−1.6		
			989	−1.9		
F_2(R, IR)	2268.6	4509	2258	−1.2	0.89	ν(CN)
			2209	−1.3		
			2228	–		
A_1(R)	2295.1	8323	2265	−1.4	0.32	ν(CN)

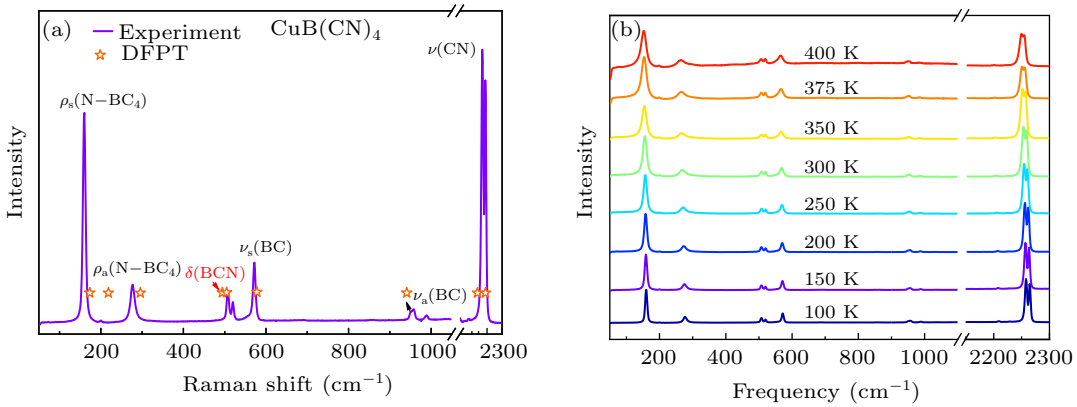


Fig. 3. (a) Unpolarized Raman spectrum measured in $CuB(CN)_4$ powder at 300 K. Stars indicate the vibrational frequency of Raman modes calculated by DFPT. The symbols ρ, δ and ν refer to rocking, in-plane bending and stretching modes, respectively; s and a indicate symmetrical and anti-symmetrical, respectively. (b) Raman spectra measured as a function of temperature from 100 K to 400 K.

Figure 3(b) shows the temperature-dependence of the Raman spectra of $CuB(CN)_4$ from 100 K to 400 K. For each Raman active mode, the frequency change with temperature has been estimated by the quantity $\frac{1}{\omega_i}\left(\frac{\partial\omega_i}{\partial T}\right)_P$ and the results are reported in Table 1. No phase transitions have been observed since no specific changes have been noted in the Raman spectra. What is instead interesting is that the all the Raman active modes show a phonon softening with temperature (Table 1). In particular, the rocking N–BC_4 modes show the largest softening while the in-plane B–C ≡ N bending δ_{BCN} modes show the lowest softening. We recall here that the temperature dependence of Raman modes includes both explicit and implicit anharmonic contributions.[44] To single out the NTE contribution of each vibrational mode at the Γ-point, Table 1 lists the Grüneisen parameters γ_i determined from our density functional perturbation theory (DFPT) calculations. All Raman active modes have positive or small negative Grüneisen parameters. Instead larger negative Grüneisen parameters at the Γ-point are exhibited by the silent F_1 modes, which are due to transverse or librational C ≡ N vibrations.

Strengthened by the fact that our DFPT calculations reproduce satisfactorily the experimental Raman modes, both

in frequency and intensity, we have calculated the phonon dispersion curves and the Grüneisen parameters in the entire Brillouin zone to further investigate the NTE mechanism of $CuB(CN)_4$ (the detailed computational methods in supporting information). Figure 4(a) shows the phonon dispersion curves calculated along the high-symmetry directions of the Brillouin zone. No negative frequencies are observed, thus indicating that $CuB(CN)_4$ is dynamically stable. In the low-frequency region (< 300 cm^{-1}), the projected density of states (PDOS) of $CuB(CN)_4$ is strongly related to the phonon vibrations of N atoms and, albeit to a lesser extent, to C and Cu atoms.

The modes Grüneisen parameters at $\Gamma(0\ 0\ 0)$ point is shown in Fig. 4(b). Due to the high symmetry of the space group, the number of phonon modes at $\Gamma(0\ 0\ 0)$ point is much smaller. One can clearly observe that there are three phonon modes with negative Grüneisen parameters: the lowest frequency phonon mode with the largest value of negative Grüneisen parameters (90 cm^{-1}, -5.6), is shown in the insert of Fig. 4(b), which displays the same vibrations direction of N and C atoms; the second one is located at 337 cm^{-1} with the opposite vibration directions of N and C atoms; the phonon mode at around 500 cm^{-1} with small negative Grüneisen parameter is corresponding to δ_{BCN} mode, it is consistent with results of temperature-dependent Raman spectra. Compared with the value of Grüneisen parameters of the same and opposite transverse vibration direction of N and C atoms, it indicates that the NTE comes from the transverse vibration direction of N and C atoms, especially the same transverse vibration ones.

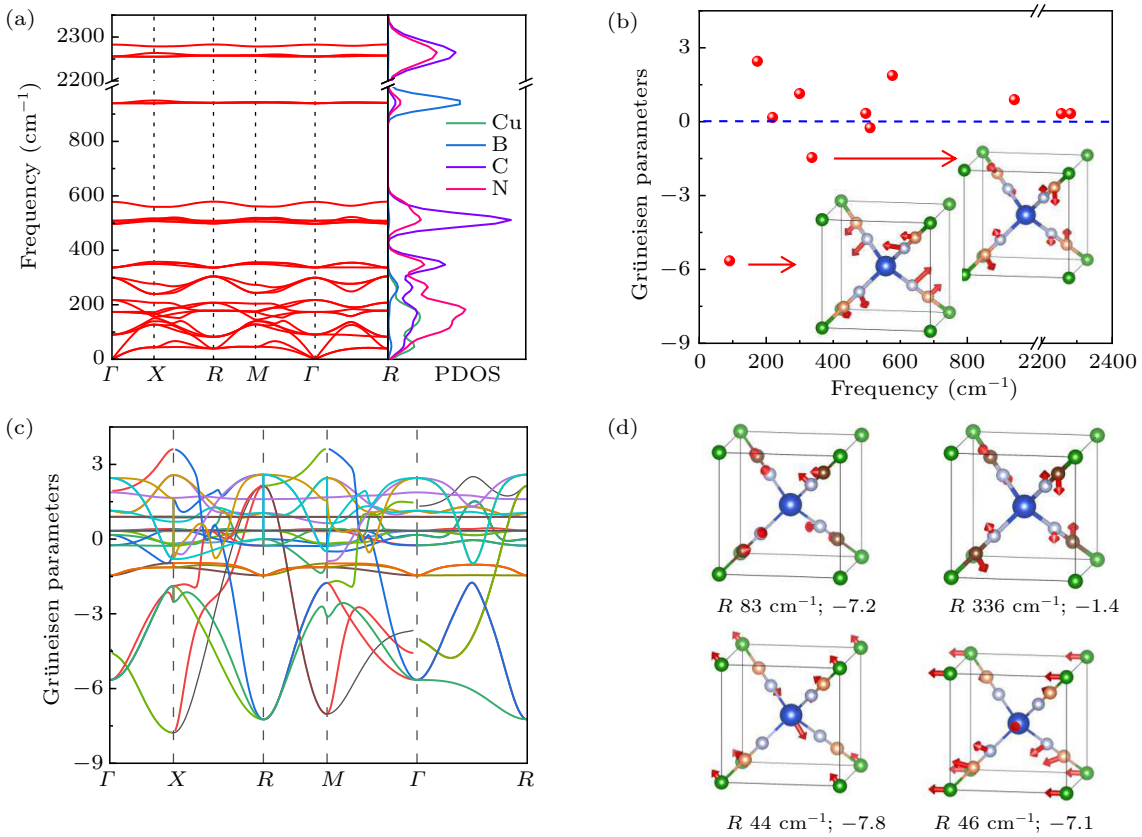


Fig. 4. (a) Calculated phonon dispersion curves and PDOS in $CuB(CN)_4$. (b) The mode Grüneisen parameters at $\Gamma(0\ 0\ 0)$ as a function of frequency. (c) Grüneisen parameters along the high-symmetry directions in the BZ. (d) Eigenvectors of selected vibrational modes with negative Grüneisen parameter. Arrows are proportional to the amplitude of the atomic motion.

However, the number of phonon modes with negative Grüneisen parameters at $\Gamma(0\ 0\ 0)$ point is still smaller than that of phonon modes with positive Grüneisen parameters. Figure 4(c) shows the mode Grüneisen parameters along all the high-symmetry directions in BZ. One can observe that the acoustic modes at $X(0.5\ 0\ 0)$ and $M(0.5\ 0.5\ 0)$ besides optical mode at $R(0.5\ 0.5\ 0.5)$ also have larger negative Grüneisen parameters. It suggests that the acoustic modes also play a critical role in driving the NTE behavior, similarly found also in other materials such as $Zn(CN)_2$,[40] Cu_2O,[45] MOF-5[22] and $Ni_2W(CN)_8$.[46] The typical eigenvectors of vibrational modes with larger negative Grüneisen parameters have been illustrated in Fig. 4(d). The vibrational mode with negative Grüneisen parameters at R point is similar to that at Γ point, while these at X and M are mainly the acoustic vibration of Cu atoms caused by the collective torsion of all atoms in $CuB(CN)_4$.

In conclusion, $CuB(CN)_4$ displays isotropic NTE and the

origin of its thermal expansion behavior has been investigated by SXRD, Raman spectroscopy and the first-principles calculations. The presence of large transverse thermal vibrations of C and N atoms is the driving force for NTE of $CuB(CN)_4$, especially those of N atoms. The analysis of the vibrational modes reveals that both the acoustic and low-frequency optical phonon modes give the main contribution to NTE. This work shed light on the NTE mechanism of $CuB(CN)_4$, a new isotropic NTE material.

Acknowledgments

This work was supported by the National Natural Science Foundation of China (Grant Nos. 22071221, 21905252, and 11774078), Natural Science Foundation of Henan Province, China (Grant No. 212300410086), and Innovation Scientists and Technicians Troop Construction Projects of Henan Province, China (No. 10094100510025). All calculations were supported by National Supercomputing Center in Zhengzhou.

References

[1] Mary T A, Evans J S O, Vogt T and Sleight A W 1996 *Science* **272** 90
[2] Sanson A 2021 *Microstructures* **11** 2021004
[3] Lind C 2012 *Materials* **5** 1125
[4] Zhang Y, Chen B, Guan D, Xu M, Ran R, Ni M, Zhou W, O'Hayre R and Shao Z 2021 *Nature* **591** 246
[5] Dove M T and Fang H 2016 *Rep. Prog. Phys.* **79** 066503
[6] Sanson A 2019 *Mater. Res. Lett.* **7** 412
[7] Mittal R, Gupta M K and Chaplot S L 2018 *Prog. Mater. Sci.* **92** 360
[8] Barrera G D, Bruno J A O, Barron T H K and Allan N L 2005 *J. Phys.: Condens. Matter.* **17** R217
[9] Attfield J P 2018 *Front. Chem.* **6** 371
[10] Coates C S and Goodwin A L 2019 *Mater. Horiz.* **6** 211
[11] Li Y, Gao Q L, Chang D H, Sun P J, Liu J Z, Jia Y, Liang E J and Sun Q 2020 *J. Phys. Condens. Mater.* **32** 455703
[12] Li M, Li Y, Wang C and Sun Q 2019 *Chin. Phys. Lett.* **36** 066301
[13] Gao Q, Chen J, Sun Q, Chang D, Huang Q, Wu H, Sanson A, Milazzo R, Zhu H, Li Q, Liu Z, Deng J and Xing X 2017 *Angew. Chem. Int. Ed.* **56** 9023
[14] Wei W, Gao Q, Guo J, Chao M, He L, Chen J and Liang E 2020 *Appl. Phys. Lett.* **116** 181902
[15] Hao Y, Xie H, Zeng G, Yuan H, Hu Y, Guo J and Liang E 2022 *Chin. Phys. B* **31** 046502
[16] Zhang M, Wang C, Zhang Y, Gao Q and Jia Y 2021 *Chin. Phys. B* **30** 056501
[17] Hu L, Chen J, Xu J, Wang N, Han F, Ren Y, Pan Z, Rong Y, Huang R, Deng J, Li L and Xing X 2016 *J. Am. Chem. Soc.* **138** 14530
[18] Gao Q, Liang E, Xing X and Chen J 2020 *J. Chinese Universities* **41** 388 (in Chinese)
[19] Chen J, Shi N, Gao Q, Sanson A, Li Q, Fan L, Ren Y, Olivi L and Xing X 2019 *Dalton T.* **48** 3658
[20] Wang J, Gao Q, Gao Y, Luo Y, Guo J, Sun Q and Liang E 2021 *Appl. Phys. Lett.* **118** 222105
[21] Goodwin A L, Calleja M, Conterio M J, Dove M T, Evans J S O, Keen D A, Peters L and Tucker M G 2008 *Science* **319** 794
[22] Gao Q, Jiao Y and Li G 2021 *Chin. Phys. B* **31** 046501
[23] Wu Y, Kobayashi A, Halder G J, Peterson V, Chapman K, Lock N, Southon P D and Kepert C 2008 *Angew. Chem. Int. Ed.* **47** 8929
[24] Yuan X, Sun Y, Guo H, Shi K, Song P, Han H, Cui J, An S, Huang R, Li L and Wang C 2021 *Mater. Design* **203** 109591
[25] Takenaka K and Takagi H 2005 *Appl. Phys. Lett.* **87** 261902
[26] Yokoyama T 2021 *Microst.* **1** 2021003
[27] Song Y, Shi N, Deng S, Xing X and Chen J 2021 *Prog. Mater. Sci.* **121** 100835
[28] Chen J, Xing X, Sun C, Hu P, Yu R, Wang X and Li L 2008 *J. Am. Chem. Soc.* **130** 1144
[29] Azuma M, Chen W t, Seki H, Czapski M, Olga S, Oka K, Mizumaki M, Watanuki T, Ishimatsu N, Kawamura N, Ishiwata S, Tucker M G, Shimakawa Y and Attfield J P 2011 *Nat. Commun.* **2** 347
[30] Xu S, Hu Y, Liang Y, Shi C, Su Y, Guo J, Gao Q, Chao M and Liang E 2020 *Chin. Phys. B* **29** 086501
[31] Chen J, Hu L, Deng J and Xing X 2015 *Chem. Soc. Rev.* **44** 3522
[32] Liang E, Sun Q, Yuan H, Wang J, Zeng G and Gao Q 2021 *Front. Phys.* **16** 53302
[33] Bridges F, Keiber T, Juhas P, Billinge S J L, Sutton L, Wilde J and Kowach G R 2014 *Phys. Rev. Lett.* **112** 045505
[34] Li C W, Tang X, Muñoz J A, Keith J B, Tracy S J, Abernathy D L and Fultz B 2011 *Phys. Rev. Lett.* **107** 195504
[35] Gao Q, Wang J, Sanson A, Sun Q, Liang E, Xing X and Chen J 2020 *J. Am. Chem. Soc.* **142** 6935
[36] Gao Q, Sun Q, Venier A, Sanson A , Huang Q, Jia Y, Liang E and Chen J 2022 *Sci. China Mater.* **65** 553
[37] Gao Y, Wang C, Gao Q, Guo J, Chao M, Jia Y and Liang E 2020 *Inorg. Chem.* **59** 18427
[38] Sanson A 2014 *Chem. Mater.* **26** 3716
[39] Hibble S J, Chippindale A M, Marelli E, Kroeker S, Michaelis V K, Greer B J, Aguiar P M, Bilbé E J, Barney E R and Hannon A C 2013 *J. Am. Chem. Soc.* **135** 16478
[40] Fang H, Dove M, Rimmer L and Misquitta A 2013 *Phys. Rev. B* **88** 104306
[41] Küppers T, Bernhardt E, Willner H, Rohm H and Köckerling M 2005 *Inorg. Chem.* **44** 1015
[42] Gao Q, Shi X, Venier A, Carnera A, Huang Q, Wu H, Chen J, Sanson A and Liang E 2020 *Inorg. Chem.* **59** 14852
[43] Bernhardt E, Henkel G and Henkel H 2000 *Z. Anorg. Allg. Chem.* **626** 560
[44] Salke N P, Gupta M K, Rao R, Mittal R, Deng J and Xing X 2015 *J. Appl. Phys.* **117** 235902
[45] Mittal R, Chaplot S, Mishra S and Bose P 2007 *Phys. Rev. B* **75** 174303
[46] Wang C, Chang D, Gao Q, Liu C, Wang Q, Huang X and Jia Y 2020 *Phys. Chem. Chem. Phys.* **22** 18655